Check for updates

Multi-slot photonic crystal cavities for high-sensitivity refractive index sensing

PEIPENG XU,[1,3,*] JIAJIU ZHENG,[2] JUN ZHOU,[1] YUEYANG CHEN,[2] CHEN ZOU,[2] AND ARKA MAJUMDAR[2,4,5]

[1]*Laboratory of Infrared Materials and Devices, Advanced Technology Research Institute, Ningbo University, Ningbo 315211, China*
[2]*Department of Electrical and Computer Engineering, University of Washington, Seattle, WA 98195, USA*
[3]*Key Laboratory of Photoelectric Detection Materials and Devices of Zhejiang Province, Ningbo, 315211, China*
[4]*Department of Physics, University of Washington, Seattle, WA 98195, USA*
[5]*arka@uw.edu*
[*]xupeipeng@nbu.edu.cn

Abstract: We present the design, fabrication, and characterization of a multi-slot photonic crystal (PhC) cavity sensor on the silicon-on-insulator platform. By optimizing the structure of the PhC cavity, most of the light can be distributed in the lower index region; thus, the sensitivity can be dramatically improved. By exposing the cavities to different mass concentrations of NaCl solutions, we obtained that the wavelength shift per refractive index unit (RIU) for the sensor is 586 nm/RIU, which is one of the highest sensitivities achieved in a non-suspended cavity. Furthermore, the size of the sensing region of the reported sensor is only 22.8 μm × 1.5 μm, making the high-sensitivity PhC cavity sensor attractive for the realization of on-chip sensor arrays.

1. Introduction

Lab-on-a-chip (LOC), which integrates many of the analytical capabilities of a biomedical research lab into a small disposable chip, can provide instant, multiplexed, and cost-effective measurements at the point of need compared with a centralized laboratory [1,2]. Photonic integrated circuit (PIC) based biosensors are ideal candidates for the LOC applications [3] due to their ability for miniaturization, extreme sensitivity, robustness, and potential for multiplexing and mass production at low cost.

Silicon photonics is an emerging chip-scale technology that has the potential to create large-scale PICs because of its compactness and compatibility with the mature CMOS technology, facilitating the fabrication of complex LOC systems [4]. There have been considerable efforts to develop different architectures of silicon photonic biosensors, including microring [5–7] and microdisk [8–10] resonators, interferometers [11–13], and one-dimensional (1D) or two-dimensional (2D) photonic crystal (PhC) microcavities [14–21]. In resonator-based architectures, a tiny change in the external refractive index can make a noticeable shift of the resonance frequencies and, thus, provide a measurable response. Among these different structures, 1D Photonic crystal (PhC) cavities are particularly intriguing in sensing community owing to their compact size and enhanced light-matter interaction due to ultra-high Q-factor and low mode volumes $\sim(\lambda/n)^3$. Hence, the total amount of analytes required to produce a measurable change in the refractive index (reflected by a change in the wavelength of the resonant peak) can be extremely tiny resulting in a very high sensitivity.

For the conventional PhC sensors, most of the electric field is confined in the core of the waveguide due to the high index contrast between silicon ($n \sim 3.46$) and its cladding, silicon dioxide ($n \sim 1.45$). In this way, only the evanescent tail of the optical mode can be utilized for

detecting analyte, which limits their sensitivity (typically ~200 nm/RIU), RIU being refractive index unit [22]. To achieve an enhanced sensitivity, slot waveguides can be used, where the discontinuity of the optical field arising at the interfaces yields an enhanced localization of the electric field inside the slot [23]. Several PhC cavities with nanogap have also been demonstrated in recent years. While the light-analyte interaction in the slotted PhC cavities is significantly improved, the achieved sensitivity is still limited (~400 nm/RIU) [15,24]. To obtain a superior sensitivity (>500 nm/RIU), suspending the PhC cavity off the substrate is required [20,25,26], which is challenging in term of fabrication complexity and robustness.

In this paper, we demonstrate a multi-slot PhC cavity (MSPhC) in silicon, which consists of four nanogaps with a width of 70 nm. Benefiting from this design, the sensitivity of the PhC sensors is highly improved. Exposing the multi-slot PhC cavities to NaCl solution with increased concentrations gives us a record high experimental bulk sensitivity of 586 nm/RIU compared with other non-suspended PhC sensors. Also, the multi-slot structure enables larger surface area around each Si post for the analyte to attach. Hence, the device can be employed to detect proteins in ultra-low concentration with the appropriate choice of antibody.
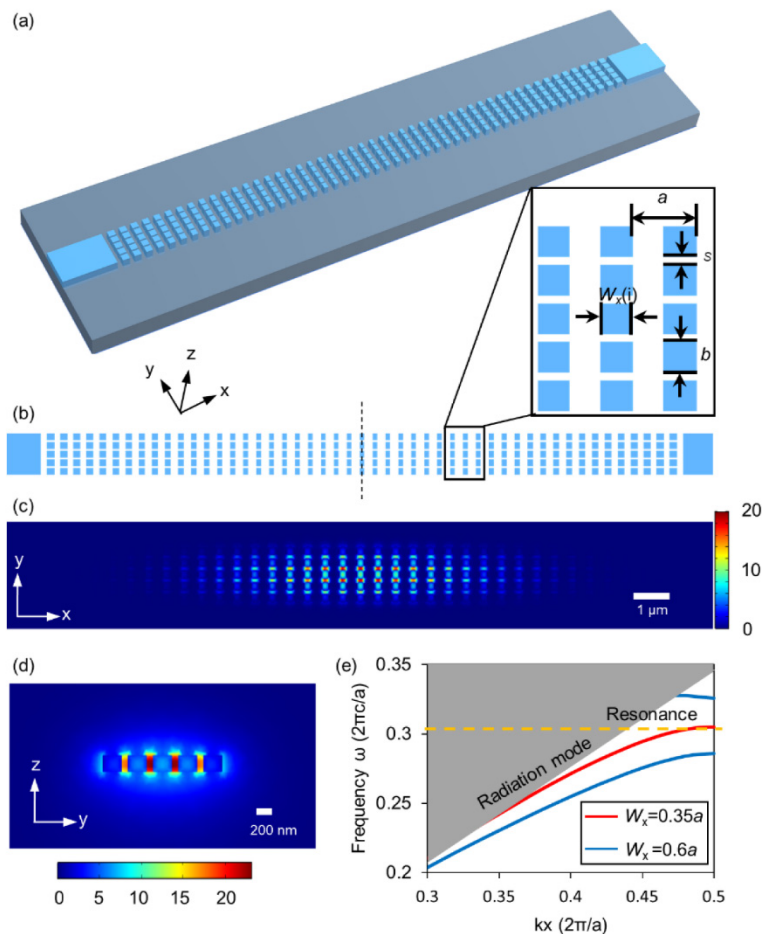
2. Design and analysis

Fig. 1. (a) Schematics of the proposed Si MSPhC device; (b) Top view of the MSPhC device. Inset: zoom-in view of the framed part. (c)-(d) The electric field ($|E|$) distribution from (c) top and (d) side taken at the center of the cavity simulated by 3D FDTD. (e) Simulated band structure of periodic multi-slot post cell (shown in the inset) with $W_x = 0.35a$ (red lines) and W_x

= 0.6a (blue lines). The yellow dashed line indicates the resonant frequency. The gray region indicates the light cone of the water.

Figure 1(a) presents the schematic of an MSPhC cavity. It consists of a 1D PhC cavity evenly split with four nanogaps in the y direction. Due to the reduced refractive index of the multi-slot scheme, the cavity possesses the combination of a weak mode confinement and a highly condensed electric filed in the slot, both of which benefit a high overlap of the optical field with the analyte. From the top view of the MSPhC cavity, shown in Fig. 1(b), the longitudinal (y-axis) length of each post and the gap between the adjacent posts are b and s, respectively. To minimize scattering loss in the propagation direction x, we keep the period a, i.e. the transverse (x-axis) distance between the posts, constant to ensure optical phase matching between adjacent unit cells [27]. To achieve a high Q-factor, the scattering perpendicular to the surface of the cavity should be reduced due to coupling to radiation modes. The scattering can be minimized when the major spatial Fourier components of the electric and magnetic field ($\int_{<\text{lightcone}>} dk(|FT(Hz)|^2 + |FT(Ez)|^2)$) are tightly localized at the edge of the first Brillouin zone [28]. To push the Fourier components toward the edge of the Brillouin zone, a convenient way is to generate a Gaussian shaped field profile within the cavity [29]. As described by Quan et al [27,30], the preferred Gaussian field profile can be achieved by linearly increasing the attenuation of the electromagnetic field from the center to the outside of the cavity (x direction). In this work, the widths of the dielectric posts are quadratically modulated from $W_x(1)$ in the center to $W_x(i_{\max})$ on the both sides, i.e. $W_x(i) = W_x(1) + (i-1)^2(W_x(i_{\max}) - W_x(1))/(i_{\max}-1)^2$ (i increases from 1 to $i_{\max}$) [15]. The MSPhC was designed using the three-dimensional finite-difference-time-domain (3D-FDTD) approach (Lumerical Solutions, Inc.) for simulations of photonic band structure and field distribution. The electric field distribution of PhC cavity from the top view is shown in Fig. 1(c). Figure 1(d) shows the cross-section view of the electric field distribution taken at the center of the PhC cavity (see cut line in Fig. 1(b)). We can find that most of the electric field of the resonant mode is strongly localized in the slot region. The band diagrams of the periodic multi-slot post cells simulated with Bloch boundary conditions with width $W_x(1) = 0.35a$ (width of the center post) and $W_x(i_{\max}) = 0.6a$ (width of the edge post) are given in Fig. 1(e). As expected, the band for the structure with $W_x(1) = 0.35a$ was higher than the one for $W_x(i_{\max}) = 0.6a$. The resonant frequency of the cavity mode [the dashed line in Fig. 1(e)] is slightly lower than the dielectric band edge of the posts with $W_x(1) = 0.35a$.

The Silicon-on-Insulator (SOI) platform with 220 nm device layer on a 3 μm thick buried silicon dioxide layer has been used in this work. The refractive index of the silicon and the silicon dioxide layer are 3.455 and 1.445 at 1550 nm, respectively. To keep the resonant wavelength of the cavity near 1550 nm, the period is chosen to be $a = 470$ nm. The effective mode volume of the MSPhC is calculated to be $2.98(\lambda/n_{Si})^3$ (defined by $V = \int dV \varepsilon |E|^2/(\varepsilon |E|^2)_{\max}$, where E is the electric field and ε is the permittivity).

Sensitivity and detection limit (defined by the minimum detectable refractive index change) are the figure of merits for a microcavity sensor. In practice, the detection limit of the sensor depends on the experimental systems including system noise, data-treating method and the quality of light sources and detectors. Hence to compare just the performance of the sensor, it is convenient to introduce the intrinsic limit of detection (iLoD) instead of the system's limit under an assumption of negligible noise, *i.e* [31]:

$$iLoD = \frac{\lambda_{\text{res}}}{Q \cdot S}, \tag{1}$$

where λ_{res} is the sensor's resonant wavelength, Q is the quality factor of the resonator, and S is the sensitivity. The sensor resolution $R = \lambda_{\text{res}}/Q$ is essentially the cavity linewidth, indicating the smallest possible spectral shift that can be accurately measured [32]. The minimum iLoD

can be reduced by the increase of the sensitivity S and Q-factor. In this work, we primarily study the dependence of sensitivity and $iLoD$ on the geometric parameters.
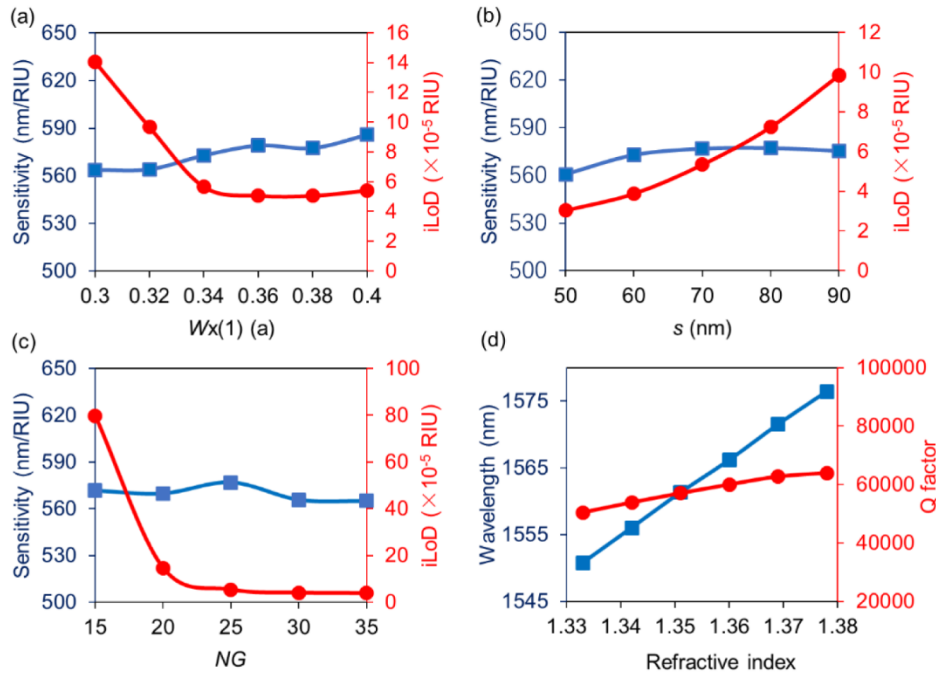

Fig. 2. Influence of (a) $W_x(0)$, (b) s and (c) number of Gaussian mirror segments (NG) on the sensitivity and $iLoD$ of multi-slot PhC cavity sensors; (d) Wavelength shift and variance of Q-factor over different background refractive indices. The sensitivity calculated in (a)-(c) is derived from the $S = \Delta\lambda/\Delta n$ with the background refractive index around 1.333.

Figures 2(a) and 2(b) show the sensitivity and $iLoD$ as a function of the center-post width $W_x(1)$ and the gap s between the adjacent posts, respectively. We find that the sensitivity of the sensor is in the range of 560~590 nm/RIU and grows slightly with the $W_x(1)$ and s, indicating that the sensitivity is only weakly dependent on $W_x(1)$ and s. In contrast, the $iLoD$ is highly sensitive to the $W_x(1)$ and s. From Fig. 2(a), the $iLoD$ stops the decreasing trend after the $W_x(1)$ reaches $0.35a$. The relationship between the $iLoD$ and the gap s is shown in Fig. 2(b). The $iLoD$ of the PhC cavity grows with the increase of s. This can be explained by the fact that PhC cavities with larger s cannot confine the optical mode well, dramatically reducing Q-factor. Considering the trade-off between the $iLoD$ and ease of fabrication, the gap is chosen as $s = 70$ nm.

For the PhC cavity, the number of the Gaussian mirrors (NG) on either side of the cavity will also influence the sensitivity and $iLoD$. Figure 2(c) shows the influence of NG on the sensitivity and $iLoD$: the $iLoD$ decreases significantly with an increase of NG and stay below 5×10^{-5} RIU when NG > 25, while the sensitivity remains almost unchanged. Since the transmittance will decrease when NG increase [27], NG is chosen to be 25 in this work to ensure a small $iLoD$ together with a measurable transmission. When $NG = 25$ on each side, the $iLoD$ is ~5×10^{-5} RIU with a cavity Q-factor more than 5×10^4.

The cavity with different post-length b is also considered to investigate its effect on sensor performance (not shown in Fig. 2). Since the portion of Si is reduced accordingly to the decrease of b, the effective index of the multi-slot waveguide will decrease. The resulting lower effective index gives rise to a weaker optical confinement, which increases both the sensitivity and the $iLoD$. As a trade-off, a 250-nm of b is chosen for each Si post.

From the above analysis, the parameters of the PhC cavity sensor are chosen to be: $a = 470$ nm, $W_x(1) = 0.35a$, $s = 70$ nm, $b = 250$ nm, and $NG = 25$ on each side. A large part of the electric field (about 50% of the total mode energy) is located in the void space, resulting in a very strong light-matter interaction between the optical field and the target analytes, and a high sensitivity. After simulating the sensor performance on different geometric parameters with the background index around 1.333, the index-dependent wavelength shifts of the PhC cavity are shown in Fig. 2(d). The simulated sensitivity of the proposed sensor is ~576 nm/RIU, and the Q-factor remains larger than 5×10^4. As our sensor cavity possesses a single mode, a large sensing range can be expected, which is especially advantageous compared to the microring-based sensors (their sensing range are inevitably limited by the free spectrum range).

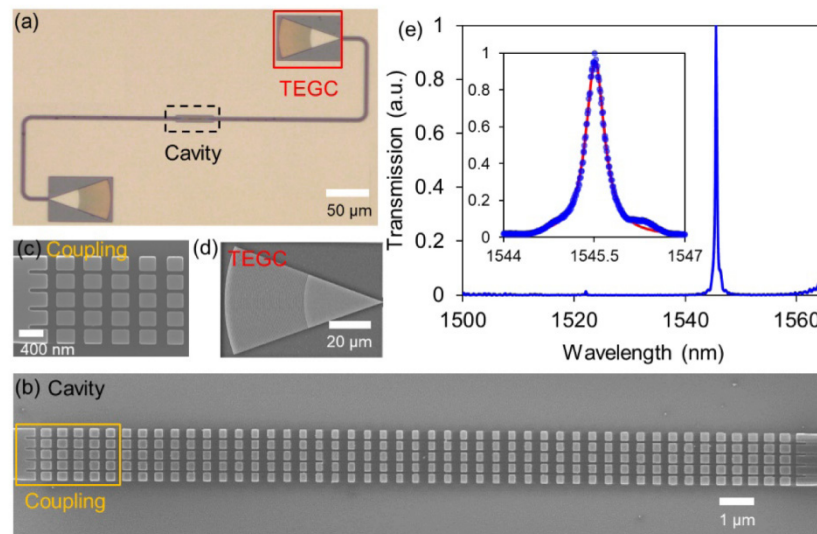## 3. Fabrication and measurement

Fig. 3. (a) Optical image of the fabricated multi-slot photonic crystal nanobeam cavity. (b), (c) SEM of the device and the enlarged view of the coupling region connecting the strip/slot waveguides. (d) SEM of the GC. (e) Measured transmission spectrum of the MSPhC cavity in 2% NaCl solution. The inset shows the fit to Lorentzian lineshape for the resonance (Q ~4200).

The device pattern was defined by direct-writing 100 keV electron-beam lithography (JEOL JBX-6300FS) using a positive tone ZEP-520A resist and transferred onto the underlying silicon layer by an anisotropic inductively coupled plasma (ICP) process utilizing a gas mixture of SF_6 and C_4F_8. To characterize the performance of the MSPhC cavity, we used appropriately designed grating couplers (GC) for TE polarization [33], as shown in Fig. 3(a). The strip waveguides with TE-type grating coupler were also fabricated on the same chip for normalization. Figures 3(b)-3(c) show the scanning electron micrographs (SEMs) of the cavity and the enlarged view of the coupling region connecting the strip/slot waveguides. Due to the high propagation loss of the multi-slot waveguide, the multi-slot region is used only in the functional part while the conventional strip waveguide is used for light propagation elsewhere. In this work, the strip waveguide with 1530-nm width is directly connected to the multi-slot waveguide (See Fig. 3(c)). Figure 3(d) shows the fully etched TE-type focusing sub-wavelength GC [33]. We probed the devices using an optical fiber setup. The polarization of the input light was controlled to match the fundamental quasi-TE mode of the waveguide by a manual fiber polarization controller (Thorlabs FPC526). A tunable continuous wave laser (Santec TSL-510) and a low-noise power meter (Keysight 81634B) were used to

measure the performance of the fabricated devices. Figure 3(e) presents the transmission spectrum of the MSPhC cavity immersed into 2% NaCl solution normalized by the peak resonance transmission. The cavity has a resonance at 1545.5 nm. Lorentzian fitting of the resonance reveals the full width at half maximum (FWHM) is about 372 pm, indicating a Q-factor of ~4200. The extinction ratio is larger than 26 dB. The quality factor is smaller than the simulated value primarily because of the water absorption at telecom wavelength range, the fabrication imperfection and scattering due to impurities in the analytes. Furthermore, we did find our device supports the high order mode, this high order mode could be well separated from the fundamental mode with its intensity much smaller than the fundamental one.

Figure 4(a) shows the measured transmission spectrum when the device is immersed in NaCl solution with different concentrations. From Fig. 4(a), we find that the resonant wavelength increases as the concentration of the NaCl solution increases. The ratio of the refractive index change to the concentration change for the aqueous solution of NaCl is about 0.0018 RIU/1% at 20°C [34]. In our experiment, the concentration varies from 0% to 5% with a step of 1%, and the corresponding refractive index ranges from 1.333 to 1.342. During the optical measurement, the temperature of the test stage was fixed at 20°C using a thermo-electric controller (TEC, TE Technology TC-720) to minimize the impact of external thermal noise and drift. After each measurement, the chip was rinsed with distilled water and agitated on a 90 °C hot plate for 10 mins to remove the residuals. As seen in Fig. 4(b), the dependence of the resonant shift on the refractive indices is linear and yields the experimental, refractive index sensitivity $S = \Delta\lambda/\Delta n = 586$ nm/RIU, which shows quite good agreement with the simulation of 576 nm/RIU. The experimental Q-factors, extracted from the fit data with different refractive indices, was in the range of 3500~4200. The measured sensitivity is the highest among all reported non-suspended cavities. The improvement factors compared to other resonators are ~2.2 for the dielectric PhC cavities (~270 nm/RIU) [21], 1.45 for the slot PhC cavities (~400 nm/RIU) [15,24], and 2.3 for the TM strip waveguides microring resonators (250 nm/RIU) [35]. Although the recently reported multi-box waveguide microring resonator possesses comparable refractive-index sensitivity to our work [36], the sensing area (22.8 × 1.5 μm^2) of our work is only 1/100 of the reported one (larger than 60 × 60 μm^2). To be used in a practical context, our compact device can be combined with microfluidic channels, which suggests strong potential for lab-on-a-chip applications [37].
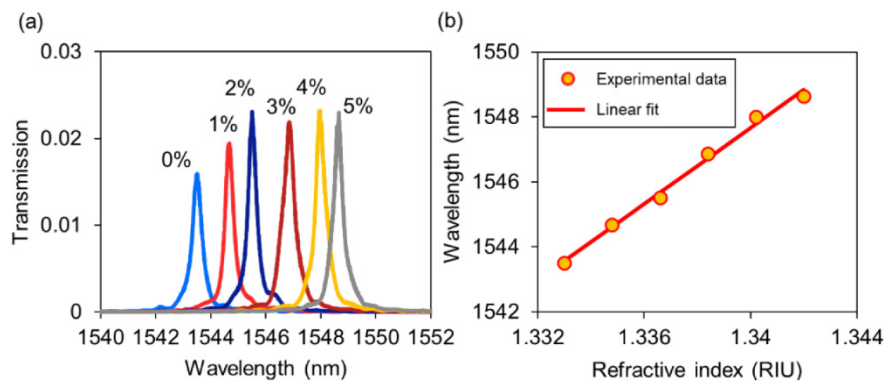

Fig. 4. (a) Measured transmission responses of the multi-slot PhC cavity immersed in the aqueous NaCl solution with different concentrations. (b) The resonant wavelength of the PhC cavity sensor as a function of the background refractive index. The sensitivity of the PhC cavity sensor is 586 nm/RIU by linear fitting.

4. Summary

In conclusion, we demonstrated a highly sensitive silicon photonic biosensor by using a novel MSPhC. The simulated and experimental results indicate that the optical power is largely congregated in the gaps between the Si posts, which significantly enhances the overlap between the optical field and analyte. The sensitivity of the PhC cavity sensor is measured by immersing the device into NaCl solution with different mass concentrations, and the sensitivity is about 586 nm/RIU, which agrees well with the simulated result. Furthermore, the total sensing area of the PhC cavity sensor is only $22.8 \times 1.5 \ \mu m^2$. The availability of such a PhC cavity with high Q-factor, high sensitivity, small size and easy fabrication, paves the way for the on-chip multiplexed sensor arrays and shed light on their applications for point-of-care medical diagnostics and high-throughput screening.

References

1. M. C. Estevez, M. Alvarez, and L. M. Lechuga, "Integrated optical devices for lab-on-a-chip biosensing applications," Laser Photonics Rev. **6**(4), 463–487 (2012).
2. J. V. Jokerst, J. W. Jacobson, B. D. Bhagwandin, P. N. Floriano, N. Christodoulides, and J. T. McDevitt, "Programmable nano-bio-chip sensors: analytical meets clinical," Anal. Chem. **82**(5), 1571–1579 (2010).
3. A. L. Washburn and R. C. Bailey, "Photonics-on-a-chip: recent advances in integrated waveguides as enabling detection elements for real-world, lab-on-a-chip biosensing applications," Analyst (Lond.) **136**(2), 227–236 (2011).
4. R. Soref, "The past, present, and future of silicon photonics," IEEE J. Sel. Top. Quantum Electron. **12**(6), 1678–1687 (2006).
5. K. De Vos, I. Bartolozzi, E. Schacht, P. Bienstman, and R. Baets, "Silicon-on-Insulator microring resonator for sensitive and label-free biosensing," Opt. Express **15**(12), 7610–7615 (2007).
6. J. Flueckiger, S. Schmidt, V. Donzella, A. Sherwali, D. M. Ratner, L. Chrostowski, and K. C. Cheung, "Sub-wavelength grating for enhanced ring resonator biosensor," Opt. Express **24**(14), 15672–15686 (2016).
7. M. Iqbal, M. A. Gleeson, B. Spaugh, F. Tybor, W. G. Gunn, M. Hochberg, T. Baehr-Jones, R. C. Bailey, and L. C. Gunn, "Label-free biosensor arrays based on silicon ring resonators and high-speed optical scanning instrumentation," IEEE J. Sel. Top. Quantum Electron. **16**(3), 654–661 (2010).
8. A. M. Armani, R. P. Kulkarni, S. E. Fraser, R. C. Flagan, and K. J. Vahala, "Label-Free, Single-Molecule Detection with Optical Microcavities," Science **317**(5839), 783–787 (2007).
9. S. M. Grist, S. A. Schmidt, J. Flueckiger, V. Donzella, W. Shi, S. Talebi Fard, J. T. Kirk, D. M. Ratner, K. C. Cheung, and L. Chrostowski, "Silicon photonic micro-disk resonators for label-free biosensing," Opt. Express **21**(7), 7994–8006 (2013).
10. X. Wang, X. Guan, Q. Huang, J. Zheng, Y. Shi, and D. Dai, "Suspended ultra-small disk resonator on silicon for optical sensing," Opt. Lett. **38**(24), 5405–5408 (2013).
11. A. Ymeti, J. Greve, P. V. Lambeck, T. Wink, S. W. van Hövell, T. A. Beumer, R. R. Wijn, R. G. Heideman, V. Subramaniam, and J. S. Kanger, "Fast, ultrasensitive virus detection using a young interferometer sensor," Nano Lett. **7**(2), 394–397 (2007).

12. K. Schmitt, B. Schirmer, C. Hoffmann, A. Brandenburg, and P. Meyrueis, "Interferometric biosensor based on planar optical waveguide sensor chips for label-free detection of surface bound bioreactions," Biosens. Bioelectron. **22**(11), 2591–2597 (2007).

13. D. Duval, A.B. González-Guerrero, S. Dante, C. Domínguez, and L.M. Lechuga, "Interferometric waveguide biosensors based on Si-technology for point-of-care diagnostic," in SPIE Photonics Europe, (2012).

14. F. Liang, N. Clarke, P. Patel, M. Loncar, and Q. Quan, "Scalable photonic crystal chips for high sensitivity protein detection," Opt. Express **21**(26), 32306–32312 (2013).

15. D. Yang, S. Kita, F. Liang, C. Wang, H. Tian, Y. Ji, M. Lončar, and Q. Quan, "High sensitivity and high Q-factor nanoslotted parallel quadrabeam photonic crystal cavity for real-time and label-free sensing," Appl. Phys. Lett. **105**(6), 063118 (2014).

16. Y. Zhang, S. Han, S. Zhang, P. Liu, and Y. Shi, "High-Q and High-Sensitivity Photonic Crystal Cavity Sensor," IEEE Photonics J. **7**(5), 1–6 (2015).

17. F. Liang and Q. Quan, "Detecting Single Gold Nanoparticles (1.8 nm) with Ultrahigh-Q Air-Mode Photonic Crystal Nanobeam Cavities," ACS Photonics **2**(12), 1692–1697 (2015).

18. D. F. Dorfner, T. Hürlimann, T. Zabel, L. H. Frandsen, G. Abstreiter, and J. J. Finley, "Silicon photonic crystal nanostructures for refractive index sensing," Appl. Phys. Lett. **93**(18), 181103 (2008).

19. D. Dorfner, T. Zabel, T. Hürlimann, N. Hauke, L. Frandsen, U. Rant, G. Abstreiter, and J. Finley, "Photonic crystal nanostructures for optical biosensing applications," Biosens. Bioelectron. **24**(12), 3688–3692 (2009).

20. B. Wang, M. A. Dündar, R. Nötzel, F. Karouta, S. He, and R. W. Heijden, "Photonic crystal slot nanobeam slow light waveguides for refractive index sensing," Appl. Phys. Lett. **97**(15), 151105 (2010).

21. K. Yao and Y. Shi, "High-Q width modulated photonic crystal stack mode-gap cavity and its application to refractive index sensing," Opt. Express **20**(24), 27039–27044 (2012).

22. E. Chow, A. Grot, L. W. Mirkarimi, M. Sigalas, and G. Girolami, "Ultracompact biochemical sensor built with two-dimensional photonic crystal microcavity," Opt. Lett. **29**(10), 1093–1095 (2004).

23. V. R. Almeida, Q. Xu, C. A. Barrios, and M. Lipson, "Guiding and confining light in void nanostructure," Opt. Lett. **29**(11), 1209–1211 (2004).

24. P. Xu, K. Yao, J. Zheng, X. Guan, and Y. Shi, "Slotted photonic crystal nanobeam cavity with parabolic modulated width stack for refractive index sensing," Opt. Express **21**(22), 26908–26913 (2013).

25. J. Jágerská, H. Zhang, Z. Diao, N. Le Thomas, and R. Houdré, "Refractive index sensing with an air-slot photonic crystal nanocavity," Opt. Lett. **35**(15), 2523–2525 (2010).

26. D. Yang, H. Tian, and Y. Ji, "High-Q and high-sensitivity width-modulated photonic crystal single nanobeam air-mode cavity for refractive index sensing," Appl. Opt. **54**(1), 1–5 (2015).

27. Q. Quan, P. B. Deotare, and M. Loncar, "Photonic crystal nanobeam cavity strongly coupled to the feeding waveguide," Appl. Phys. Lett. **96**(20), 203102 (2010).

28. K. Srinivasan and O. Painter, "Momentum space design of high-Q photonic crystal optical cavities," Opt. Express **10**(15), 670–684 (2002).

29. Y. Akahane, T. Asano, B.-S. Song, and S. Noda, "High-Q photonic nanocavity in a two-dimensional photonic crystal," Nature **425**, 944 (2003).

30. Q. Quan and M. Loncar, "Deterministic design of wavelength scale, ultra-high Q photonic crystal nanobeam cavities," Opt. Express **19**(19), 18529–18542 (2011).

31. T. Yoshie, L. Tang, and S.-Y. Su, "Optical Microcavity: Sensing down to Single Molecules and Atoms," Sensors (Basel) **11**(2), 1972–1991 (2011).

32. I. M. White and X. Fan, "On the performance quantification of resonant refractive index sensors," Opt. Express **16**(2), 1020–1028 (2008).

33. Y. Wang, X. Wang, J. Flueckiger, H. Yun, W. Shi, R. Bojko, N. A. Jaeger, and L. Chrostowski, "Focusing sub-wavelength grating couplers with low back reflections for rapid prototyping of silicon photonic circuits," Opt. Express **22**(17), 20652–20662 (2014).

34. C.-Y. Tan and Y.-X. Huang, "Dependence of Refractive Index on Concentration and Temperature in Electrolyte Solution, Polar Solution, Nonpolar Solution, and Protein Solution," J. Chem. Eng. Data **60**(10), 2827–2833 (2015).

35. S. TalebiFard, S. Schmidt, W. Shi, W. Wu, N. A. Jaeger, E. Kwok, D. M. Ratner, and L. Chrostowski, "*Optimized sensitivity* of Silicon-on-Insulator (SOI) strip waveguide resonator sensor," Biomed. Opt. Express **8**(2), 500–511 (2017).

36. E. Luan, H. Yun, L. Laplatine, Y. Dattner, D. M. Ratner, K. C. Cheung, and L. Chrostowski, "Enhanced Sensitivity of Subwavelength Multibox Waveguide Microring Resonator Label-Free Biosensors," IEEE J. Sel. Top. Quantum Electron. **25**(3), 1–11 (2019).

37. C. Monat, P. Domachuk, and B. J. Eggleton, "Integrated optofluidics: a new river of light," Nat. Photonics **1**, 106 (2007).